JGR Biogeosciences

RESEARCH ARTICLE
10.1029/2023JG007479

Key Points:

- Size and density fractionation of sediment organic carbon (OC) reveals substantial contrasts between different fractions and environments
- OC- and biomarker loading shows that a significant amount of terrestrial OC is lost along a land-ocean transect
- Combining methods in dynamic environments such as the nearshore zone is key in studying the fate of permafrost OC

Correspondence to:
D. Jong and J. Vonk,
d.j.jong@vu.nl;
j.e.vonk@vu.nl

Citation:
Jong, D., Bröder, L., Tesi, T., Tanski, G., Oudenhuijsen, M., Fritz, M., et al. (2024). Selective sorting and degradation of permafrost organic matter in the nearshore zone of Herschel Island (Yukon, Canada). *Journal of Geophysical Research: Biogeosciences*, *129*, e2023JG007479. https://doi.org/10.1029/2023JG007479

Received 14 MAR 2023
Accepted 20 NOV 2023

Selective Sorting and Degradation of Permafrost Organic Matter in the Nearshore Zone of Herschel Island (Yukon, Canada)

Dirk Jong[1], Lisa Bröder[1,2], Tommaso Tesi[3], George Tanski[1,4], Mickolai Oudenhuijsen[1], Michael Fritz[4], Hugues Lantuit[4,5], Negar Haghipour[2], Timothy Eglinton[2], and Jorien Vonk[1]

[1]Department of Earth Sciences, Vrije Universiteit Amsterdam, Amsterdam, The Netherlands, [2]Geological Institute, Swiss Federal Institute of Technology (ETH), Zürich, Switzerland, [3]CRN, Institute of Polar Sciences, Bologna, Italy, [4]Alfred Wegener Institute Helmholtz Centre for Polar and Marine Research, Potsdam, Germany, [5]Institute for Geosciences, University of Potsdam, Potsdam, Germany

Abstract Erosion of permafrost coasts due to climate warming releases large quantities of organic carbon (OC) into the Arctic Ocean. While burial of permafrost OC in marine sediments potentially limits degradation, resuspension of sediments in the nearshore zone potentially enhances degradation and greenhouse gas production, adding to the "permafrost carbon feedback." Recent studies, focusing on bulk sediments, suggest that permafrost OC derived from coastal erosion is predominantly deposited close to shore. However, bulk approaches disregard sorting processes in the coastal zone, which strongly influence the OC distribution and fate. We studied soils and sediments along a transect from the fast-eroding shoreline of Herschel Island—*Qikiqtaruk* (Yukon, Canada) to a depositional basin offshore. Sample material was fractionated by density (1.8 g cm^{-3}) and size (63 μm), separating loose OC from mineral-associated OC. Each fraction was analyzed for element content (TOC, TN), carbon isotopes ($\delta^{13}C$, $\Delta^{14}C$), molecular biomarkers (*n*-alkanes, *n*-alkanoic acids, lignin phenols, cutin acids), and mineral surface area. The OC partitioning between fractions changes considerably along the transect, highlighting the importance of hydrodynamic sorting in the nearshore zone. Additionally, OC and biomarker loadings decrease along the land-ocean transect, indicating significant loss of OC during transport. However, molecular proxies for degradation show contrasting trends, suggesting that OC losses are not always well reflected in its degradation state. This study, using fraction partitioning that crosses land-ocean boundaries in a way not done before, aids to disentangle sorting processes from degradation patterns, and provides quantitative insight into losses of thawed and eroded permafrost OC.

Plain Language Summary The Arctic coastline is vulnerable for erosion, since it mostly consist of permafrost (permanently frozen ground), which undergoes rapid warming due to climate change. Thaw and erosion of permafrost along the coast releases organic carbon (OC), that has been stored for millennia, into the ocean. There, in the ocean, this carbon can be degraded back into CO_2, potentially enforcing climate warming, or it can settle to the sediments, and potentially be stored again for millennia. The permafrost and the sediment consist of particles, for example, sand, silt, and clay, and loose fragments of vegetation. In this study, we separated the OC that is associated with fine particles (silt and clay) from the loose fragments of organic matter. We observe that these two fractions of sediment have a very different composition and source, and end up somewhere else in the marine system. This study further shows that a large part of the OC associated with minerals (silt and clay) is lost during transport, but also that indicators for degradation show contrasting results. Overall, we highlight the importance of looking at sediment fractions separately, and also emphasize studying the transitional zone between land to ocean for the permafrost carbon cycle.

1. Introduction

The Arctic experiences widespread warming at an accelerated rate, currently three times faster than the global average (IPCC, 2021). This accelerated warming causes permafrost, the permanently frozen ground, to thaw and destabilize. Permafrost soils contain approximately 1,300 Pg of OC (Hugelius et al., 2014), which, when released upon thaw, impact aquatic systems such as rivers, lakes and marine coastal areas. Furthermore, decomposition of remobilized permafrost OC causes release of greenhouse gases CO_2 and CH_4 to the atmosphere, potentially enhancing climate warming, a positive feedback mechanism referred to as the "permafrost carbon feedback"

(Schuur et al., 2015). In contrast, deposition and storage of permafrost OC in river- and marine sediments attenuates this feedback due to long term burial of OC.

The Arctic is becoming increasingly vulnerable to coastal erosion, due to the extended open water season and increased frequency of storms caused by climate warming, and due to the unconsolidated and ice-rich nature of over 65% of the Arctic coastline (Günther et al., 2015; Lantuit et al., 2012; Overeem et al., 2011). Increased erosion rates means an increase in export of permafrost-derived OC from coastal areas to the open ocean. During this cross-shelf transport of permafrost OC, it is vulnerable to oxidative degradation. Multiple studies have investigated loss of permafrost-derived OC during cross-shelf transport (e.g., Bröder et al., 2019; Goñi et al., 2005; Vonk et al., 2010), however, only a few studies have looked into the behavior of permafrost OC in transitional environments between the terrestrial and marine realm, for example, river delta's, estuaries and the nearshore zone (Grotheer et al., 2020; Jong et al., 2020, 2023; Tanski et al., 2017; Winterfeld et al., 2015a, 2015b). The Arctic nearshore zone is a very dynamic system, strongly influenced by waves, tides and currents, however, it remains relatively under-studied due to logistical constraints, as it is either too shallow to reach with research vessels and/or too remote to access by land (Fritz et al., 2017).

To study such a dynamic system, methods need to be developed and applied to objectively compare soil and sediment samples from different energetic environments. Sedimentological analyses need to be combined with techniques to characterize OC (i.e., $\delta^{13}C$ and $\Delta^{14}C$ isotopic signature and terrestrial biomarker proxies). For example, transport, sorting and winnowing of sediment moving through the nearshore zone to a sedimentary basin introduces a trend from coarse sediment nearshore, to fine sediment in the offshore basin (e.g., Jong et al., 2020; Radosavljevic et al., 2022). As we know from previous studies (e.g., Tesi et al., 2016), different types of OC have affinity for- or are preferentially deposited with certain fractions of sediment. Organic debris, that is, loose particles of vegetation, woody material, or other organic tissue, are often coarse enough to settle rapidly, together with (fine) sand. In contrast, mineral bound OC is mostly attached to silt and clay, and can be transported further offshore. Since both of these OC "pools" have entirely different chemical composition and potential for degradation, it is impossible to disentangle sorting from degradation processes comparing bulk sediment between different environments. Sediment fractionation methods provide an opportunity here. Multiple fractionation strategies are possible, some better fit for in situ soil studies and some better fit for dynamic sedimentary systems: on size only (e.g., Bao et al., 2019; Coppola et al., 2007; Freymond et al., 2018), with multiple density steps (e.g., Wakeham et al., 2009), or a combination of size and density (Höfle et al., 2013; Tesi et al., 2016). In this study we will be using a combined approach, since in aquatic sedimentary environments deposition of particles is depended on both size and density (Stokes law).

To study degradation of organic matter (OM), a variety and/or combination of methods can be used. For example, the C/N ratio and $\delta^{13}C$ have often been used to discern types of OM, usually between terrestrial plant material and marine algae, but also between fresh vegetation versus more degraded soil OM (Meyers, 1994; Strauss et al., 2015). Generally, fresh terrestrial vegetation has a low $\delta^{13}C$ value ($<-25‰$), but a high C/N ratio (C/N ratio >20), while soil OM shares the low $\delta^{13}C$, but generally has a lower C/N ratio due to degradation and thus removal of carbon (Meyers, 1994). On the other hand, marine primary production generally has a higher $\delta^{13}C$ ($<22‰$) and a much lower C/N ratio (4–10) (Meyers, 1994). In a similar fashion, the high molecular weight *n*-alkanoic acid to *n*-alkane ratio, and the cutin to lignin ratio can also be used to discern between fresh vegetation OM and soil OM. Lipid biomarkers such as cutin, *n*-alkanoic acids and *n*-alkanes typically have a higher affinity for mineral particles due to adsorption and desorption processes, thus being more enriched in soil and sediments, while lignin generally has a much higher concentration in organic debris/plant fragments (Höfle et al., 2013; Tesi et al., 2010, 2016).

The combination of sediment fractionation methods and biogeochemical proxies for degradation provides a powerful tool to assess sorting and degradation processes on specific fractions of sediment OC. We will use this strategy to give insight into the processes affecting (permafrost) OC on three specific sediment fractions along a land-to-ocean transect following this material from thawing permafrost, through a dynamic "disturbed zone" and the nearshore zone, to an enclosed basin offshore Herschel Island—*Qikiqtaruk*.

2. Methods

2.1. Study Area

Herschel Island—*Qikiqtaruk* is an island in the Beaufort Sea in the western Canadian Arctic (N 69.60°; W 139.00°, Figure 1b), to the West of the Mackenzie River delta. The island is mainly composed of ice-rich continuous

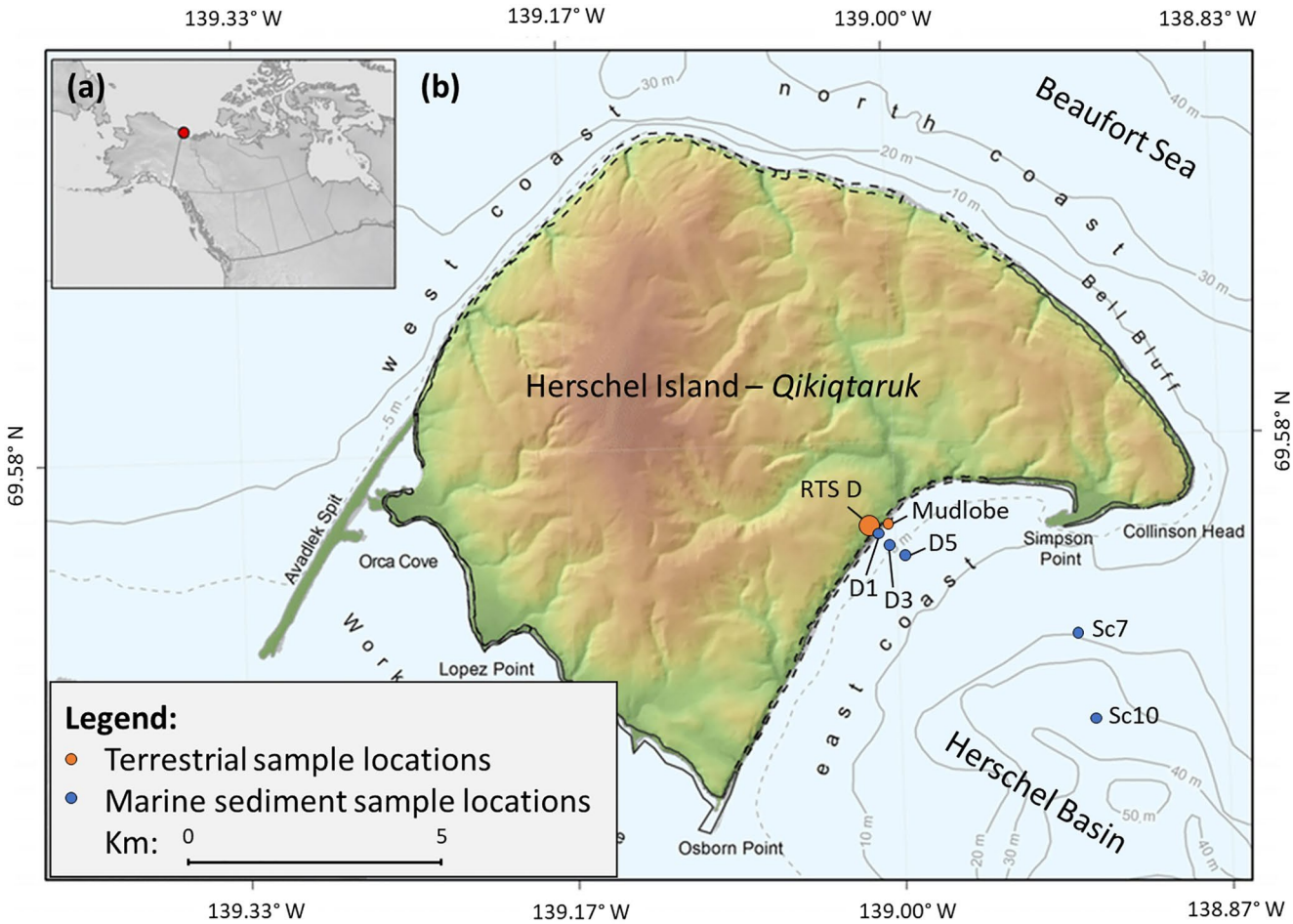

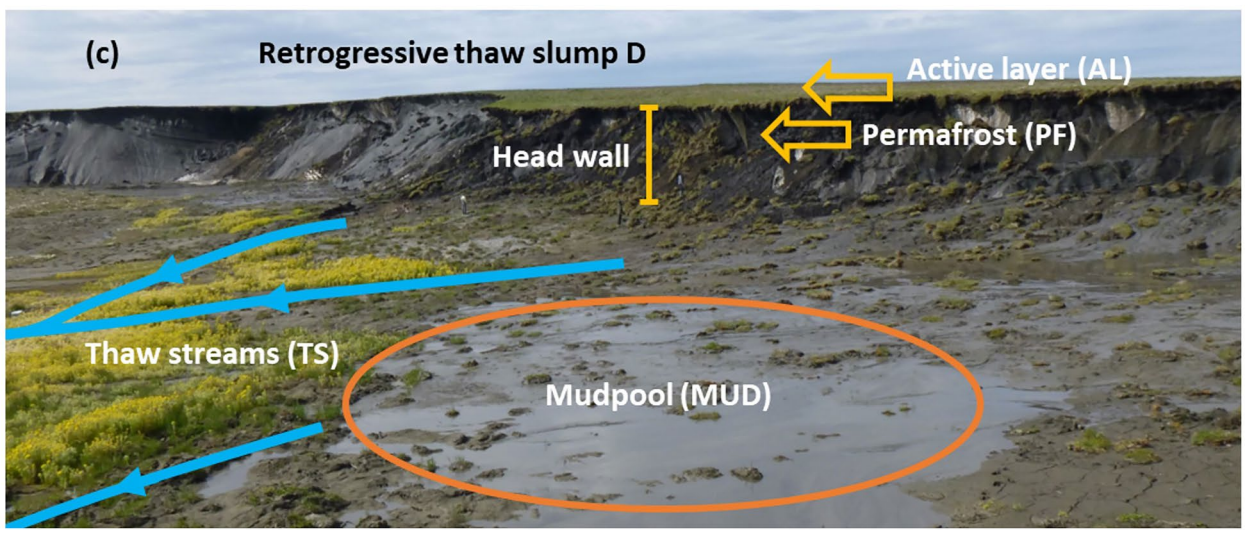

Figure 1. Map with sample locations. (a) Canada and Alaska showing the location of Herschel Island—*Qikiqtaruk*, (b) Herschel Island and basin with the location of retrogressive thaw slump D (RTS D), the location of the mudlobe sample, and the locations of the marine sediment samples. Adapted from Obu et al. (2016). (c) Photo of RTS D, highlighting the features that were sampled within the slump. The coast is to the left, just outside of the frame. Head wall is approximately 12 m high at the location of the yellow bar.

Table 1
Sample Details: Full Sample Name, Short Sample identifier as Used in the Text and Figures, the Environmental Zone or Category of the Sample, Location, Sampling Date and Water Depth of the Marine Sediment Samples

Sample name	Sample ID	Zone/category	Latitude (°)	Longitude (°)	Date (dd/mm/yyyy)	Water depth (m)
SLPD17-Al-mid-01	AL_01	Active layer	69.57151	−139.01526	31/07/2017	
SLPD17-Al-mid-02	AL_02	Active layer	69.57155	−139.01582	31/07/2017	
SLPD17-Pf-01	PF_01	Permafrost	69.57147	−139.01514	20/07/2017	
SLPD17-Pf-03	PF_03	Permafrost	69.57147	−139.01514	20/07/2017	
SLPD17-Mud-03	Mud_03	Disturbed	69.57120	−139.01582	31/07/2017	
SLPD17-Mud-04	Mud_04	Disturbed	69.57120	−139.01582	31/07/2017	
YC17_SlpD_TS_06	TS_06	Disturbed	69.56799	−139.01003	31/07/2017	
YC17-SLPD-MUDLOBE	Mudlobe	Disturbed	69.56949	−139.00596	31/07/2017	0
YC17_D1_SED	D1	Nearshore	69.56790	−139.00999	24/07/2017	0.6
YC17_D3_SED	D3	Nearshore	69.56584	−139.00508	24/07/2017	4.8
YC17_D5_SED	D5	Basin	69.56386	−138.99764	24/07/2017	7.7
PG2311-1 Sc10 0–3 cm	Sc10	Basin	69.55227	−138.92223	01/05/2016	20
PG2308-1 Sc7 0–3 cm	Sc7	Basin	69.54073	−138.91689	01/05/2016	37

permafrost, which was an ice-thrust moraine formed by the Laurentide Ice Sheet during the Late Wisconsin, and consists of glacially reworked marine and terrestrial sediments (Fritz et al., 2012; Rampton, 1982). Due to the ice-rich composition and its formation history, the island experiences high rates of coastal erosion, on average 0.7 m per year, but with extremes of 14–22 m per year at retrogressive thaw slumps (RTS) and coastal permafrost bluffs on the south-eastern side of the island (Irrgang et al., 2018; Obu et al., 2017).

The rapid coastal erosion of Herschel Island—*Qikiqtaruk* mobilizes large amounts of OC-rich sediments (Fritz et al., 2012; Obu et al., 2016), this sediment is concentrated in the Herschel Basin, an enclosed sedimentary basin on the south-eastern side of Herschel Island—*Qikiqtaruk*. The Herschel Basin is approximately 7 by 18 km, has a maximum water depth of 75 m, and the majority of the basin sediments originate from local coastal erosion (Grotheer et al., 2020). Particulate matter derived from coastal erosion is deposited relatively close to shore (Jong et al., 2020; Klein et al., 2019). The ice-free season lasts from June to September, during this period the Mackenzie River outflow causes a brackish upper mixed layer of 5–10 m deep, which reaches the eastern shore of Herschel Island (Doxaran et al., 2012; Macdonald & Yu, 2006). The tidal range is small in this part of the Arctic Ocean (<0.5 m), however, storm surges can raise the sea water level by several meters (Harper, 1990).

2.2. Sample Acquisition and Description

Sediment, soil and permafrost samples were taken along a transect from the source (undisturbed active layer and permafrost), via two transitional zones (a terrestrial disturbed zone, i.e., the "scar zone" of the RTS, and the marine nearshore zone up to a water depth of 5 m), to sink (basin sediment, water depth >20 m) at the coast of Herschel Island—*Qikiqtaruk* and the (semi-enclosed) Herschel Basin in Yukon, Canada, just west of the Mackenzie River delta (Figure 1; Table 1).

For the terrestrial samples, taken at a large thaw slump labeled "RTS-D" (Figures 1c, 1e, and 1g. Tanski et al., 2017), four permafrost (PF) and active layer (AL) samples were selected to represent the "undisturbed" terrestrial material, and four samples from the scar zone and thaw stream (TS) were selected to represent the "disturbed" material. For the undisturbed terrestrial material, and two permafrost samples were taken from the head wall of the thaw slump, approximately one m below the AL, with a rotary drill (ø 10 cm), and two samples were taken of the overlying AL (at approximately 30 cm soil depth).

The "disturbed" terrestrial material is a thawed and mobilized mixture of AL and permafrost material across the whole stratigraphic column of the RTS. These samples thus represents a mixture of all mobilized strata. Classification of the disturbed samples follows Tanski et al. (2017). Two samples were collected at a "mudpool" close

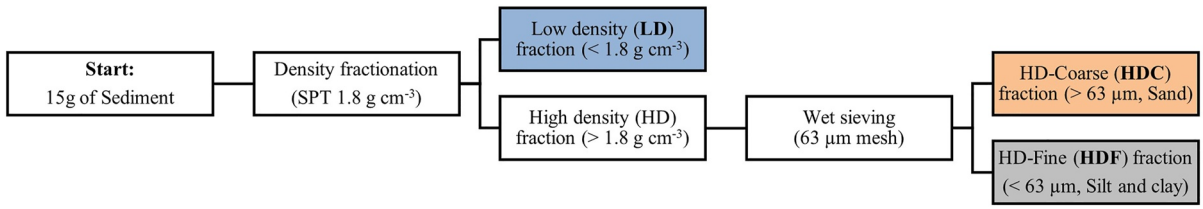

Figure 2. Flow chart of sediment fractionation method, including density fractionation with a sodium polytungstate solution of 1.8 g cm^{-3} to separate the low density from the high density (HD) fraction, and wet-sieving over a 63 µm mesh to separate fine (HDF) from course (HDC) HD material. The color coding of the fractions corresponds to Figures 3, 4, 5a, and 6.

to the head wall of the thaw slump, one sample was taken from a TS draining these mudpools, and one sample was taken at a "mudlobe" at the coast where the material from the TS was (temporarily) deposited before being washed into the marine system. For the TS sample, one L of TS mud was filtered through a 90 mm, 0.2 µm PES (polyethersulfone) membrane filter in a stainless steel filter unit and material was carefully scraped off the filter.

For the marine samples, three marine surface (0–5 cm deep) sediment samples were taken in July 2017 with a stainless-steel Van Veen grab sampler on a transect perpendicular to the Herschel coast, staring at RTS D. The two shallowest samples (at 0.6 and 4.8 m water depth) were above the marine surface mixed layer, that is, the "resuspension zone" (Jong et al., 2020), and are considered "disturbed marine" in this study. The deeper sample (7.7 m) was classified as "deposition zone" following Jong et al. (2020). The three nearshore grab samples were supplemented with surface sediment (0–3 cm) of two short cores taken from Herschel Basin with an UWITEC gravity corer, in May 2016, extending the transect into the deepest part of the basin, at water depths of 20.4 and 36.7 m (Grotheer et al., 2020). All samples were freeze dried, homogenized, and a 15 g split was taken for the further analyses of this study.

2.3. Sediment Density and Size Fractionation

The samples were fractionated by density with an aqueous (MilliQ) solution of sodium polytungstate (SPT; $Na_6[H_2W_{12}O_{40}]$; TC-Tungsten Compounds GmbH), with a density of 1.8 g cm^{-3}, followed by size fractionation through wet-sieving over a 63 µm mesh (Figure 2). The fractionation protocol and density cut-off were based on Tesi et al. (2016) and Wakeham et al. (2009). Centrifuge vials of 50 mL were filled with approximately 15 g of sediment and 45 mL of SPT solution. The sediment was first suspended with a vortex mixer, then sonicated in an ultrasonic bath for 2 min, and after sonication shaken by hand, and vortexed again to evenly suspend all particles in the SPT solution. The samples were centrifuged at 18,000 relative centrifuge force for 30 min to separate the low-density (low density (LD), <1.8 g cm^{-3}) and high-density (high density (HD), >1.8 g cm^{-3}) fractions. After centrifugation, supernatant containing the LD fraction was gently decanted from the centrifuge tubes and filtered with a 0.45 µm nylon membrane in a pre-cleaned glass filtering unit. These steps were repeated 6 to 8 times until the supernatant was clear.

The LD fraction on the filter was rinsed with MilliQ to remove SPT, and rinsed from the filter into a centrifuge tube. This fraction was then frozen, freeze dried and weighed afterward. The HD fraction left in the centrifuge tube was rinsed once with MilliQ water to remove the SPT solution before wet sieving. The HD fraction was sieved through a 63 µm mesh with 400–800 mL of demineralized water, which was collected in a 1 L glass beaker. The HD-Coarse (>63 µm; HDC) fraction was rinsed from the sieve into a new 50 mL centrifugation tube, the HD-Fine (<63 µm; HDF) fraction was concentrated from 400—800 mL to approximately 50 mL by repeated centrifugation, decanting the supernatant. Both HD fractions were frozen, freeze dried and weighed. The average recovery of the fractionation procedure was 92.1 ± 3.5% (n = 13).

2.4. Mineral Surface Areal Analyses

For mineral surface area (SA) measurements, the 6-point Brunauer–Emmett–Teller (BET) nitrogen adsorption method was used to measure the specific SA of the sediment samples (Brunauer et al., 1938). Subsamples of about 1.5 g of the two HD fractions were combusted at 450°C for 12 hr to remove OC, rinsed twice with MilliQ to remove salt and ashes, and freeze dried. Directly prior to analysis, the samples were degassed at 300°C under

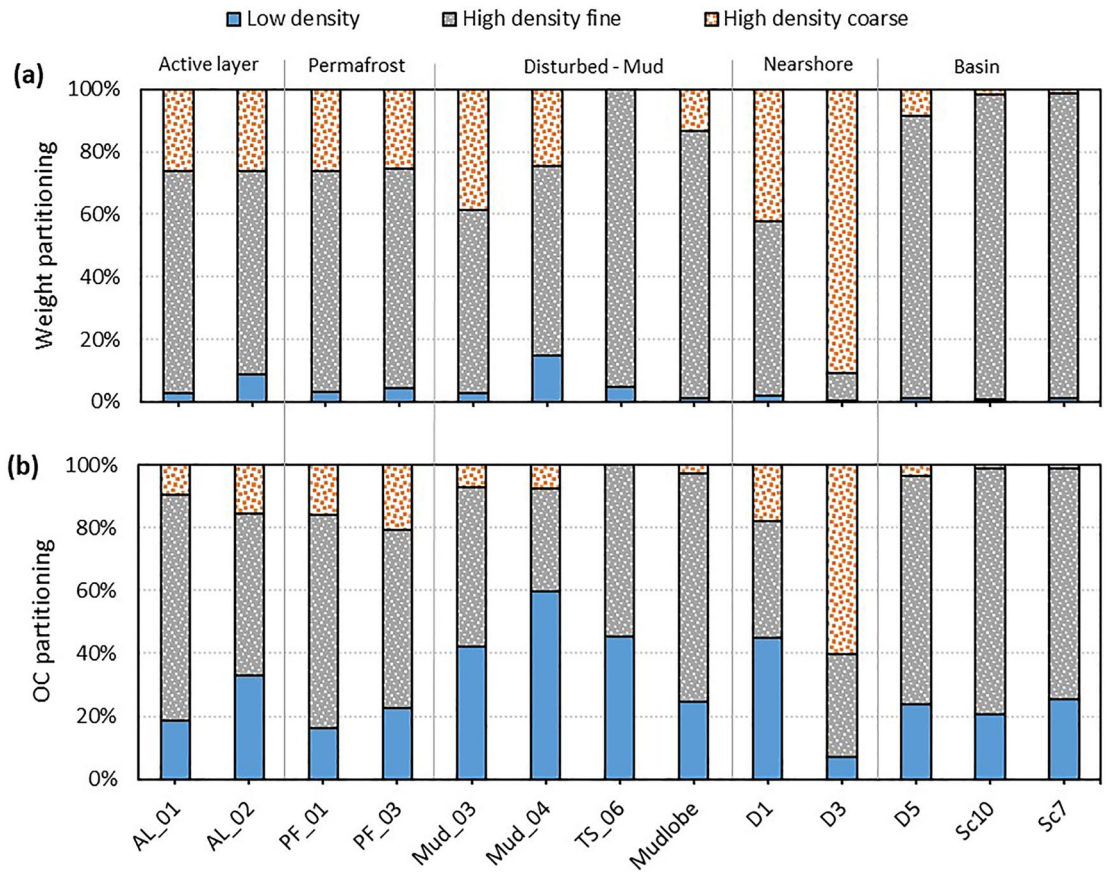

Figure 3. (a) Weight partitioning (% of the total sample weight) in land, nearshore and basin of the high density (HD) fine (<63 μm >1.8 g cm^{-3}), HD coarse (>63 μm > 1.8 g cm^{-3}) and low density (<1.8 g cm^{-3}) sediment fractions along the transect from land to ocean. (b) organic carbon (OC) partitioning (% of total OC of the sample) of the fractions, based on the total organic carbon content (% OC) for each separate fraction and its weight partitioning.

vacuum and measured with a Quantachrome Nova 4200e SA analyzer. SA measurements were checked against two certified reference materials (of 5.41 and 27.46 m^2 g^{-1}).

2.5. Bulk Geochemical Analyses

2.5.1. Total Organic Carbon, Nitrogen & Stable Carbon Isotope Analyses

All sediment fractions were subsampled and weighed into pre-combusted silver capsules for total organic carbon (TOC), total nitrogen (TN) and for $\delta^{13}C$ analyses. The LD fraction was ground and homogenized using an agate mortar and subsequently subsampled. Inorganic C was removed from the subsamples by fumigation in a desiccator with 37% HCl (at 60°C for 72 hr; Komada et al., 2008). Afterward, samples were dried over NaOH (at 60°C for 48 hr) to neutralize any remaining acid. The silver capsules were wrapped in tin boats to aid combustion. The ^{13} C values are reported following the δ notation relative to the Vienna Pee Dee Belemnite (VPDB) standard. TOC and TN were measured on an elemental analyzer at the National Research Council Institute of Polar Sciences (Bologna, Italy). The $\delta^{13}C$ values were determined by isotope-ratio mass spectrometry (IRMS; Thermo Finnigan Delta XP) coupled to a Conflo III and a Flash Elemental Analyzer 1112 at the Stable Isotope laboratory of the Vrije Universiteit Amsterdam, and checked against an internal control standard (error of <0.1‰).

2.5.2. Radiocarbon

Radiocarbon analyses ($\Delta^{14}C$) were done at the Laboratory of Ion Beam Physics of the Swiss Federal Institute of Technology (Zürich, Switzerland), using a MICADAS accelerator mass spectrometer following McIntyre et al. (2017). Subsamples of the fractionated sedimentwere weighed into pre-combusted silver capsules, and

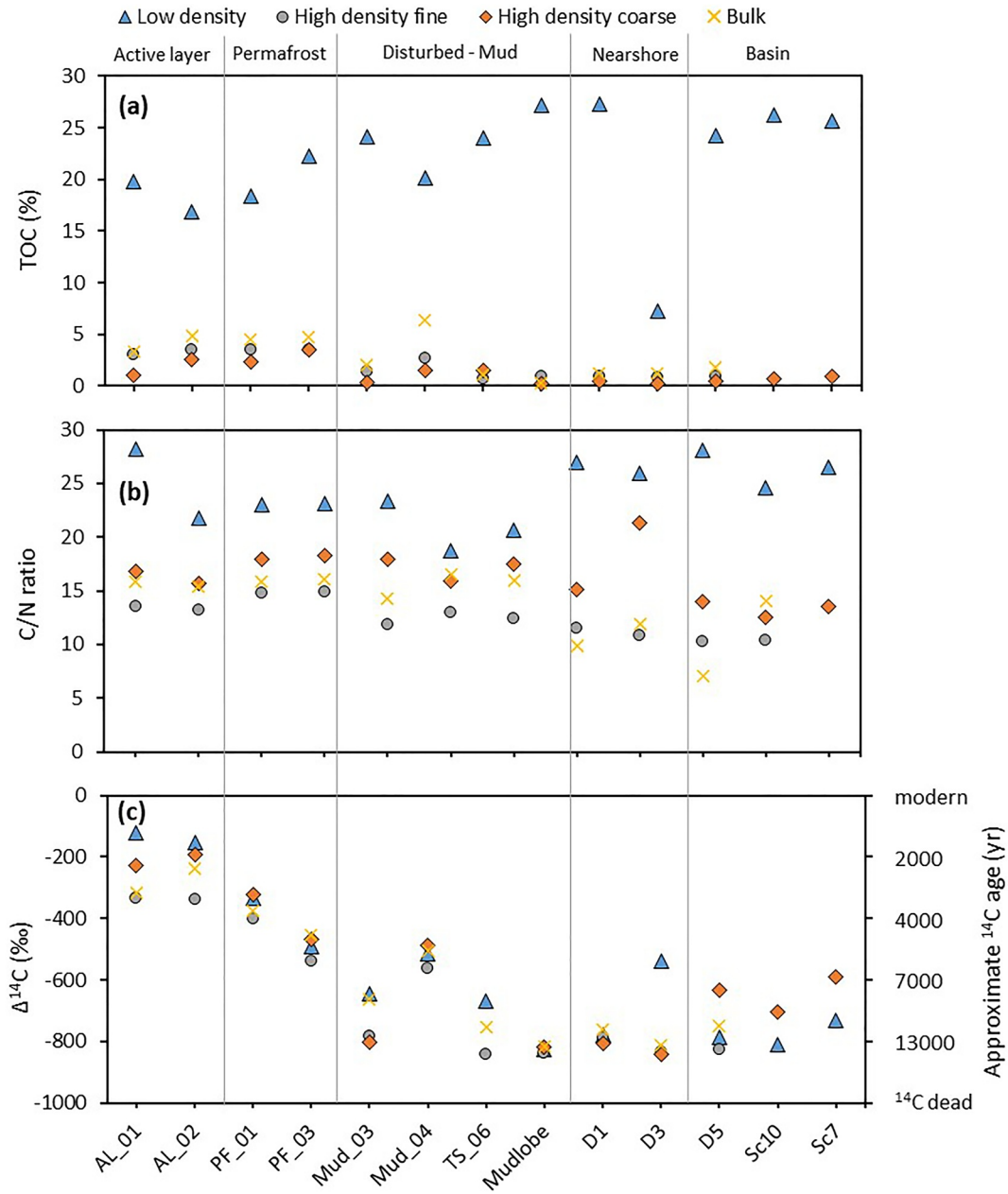

Figure 4. Total organic carbon (TOC) content, carbon to nitrogen ratio (C/N), and radiocarbon ($\Delta^{14}C$) in land, nearshore and basin sediment fractions along the transect from land to ocean. In yellow crosses for comparison the bulk TOC% as measured by previous studies (Fritz et al., 2012; Grotheer et al., 2020; Jong et al., 2020). (a) TOC (%) of the high density (HD) fine (<63 μm >1.8 g cm^{-3}), HD coarse (>63 μm > 1.8 g cm^{-3}) and low density (<1.8 g cm^{-3}) fractions. (b) Same for the carbon to nitrogen ratio (elemental), and (c) $\Delta^{14}C$ ratio (‰), with less negative values representing younger OC, and more negative values older OC. The right *y*-axis shows the approximate ^{14}C ages for reference (log scale). 'Modern' means after 1950, '^{14}C dead' means more than 50,000 years old.

inorganic C was removed by fumigation in a desiccator similar to described in Section 2.5.1. Samples were wrapped in tin capsules after fumigation. The radiocarbon results were corrected for background contamination using the method described in Haghipour et al. (2018). The radiocarbon data in this paper is presented either as $\Delta^{14}C$ (‰) or as conventional (uncalibrated) radiocarbon age (yr.) (Stuiver & Polach, 1977).

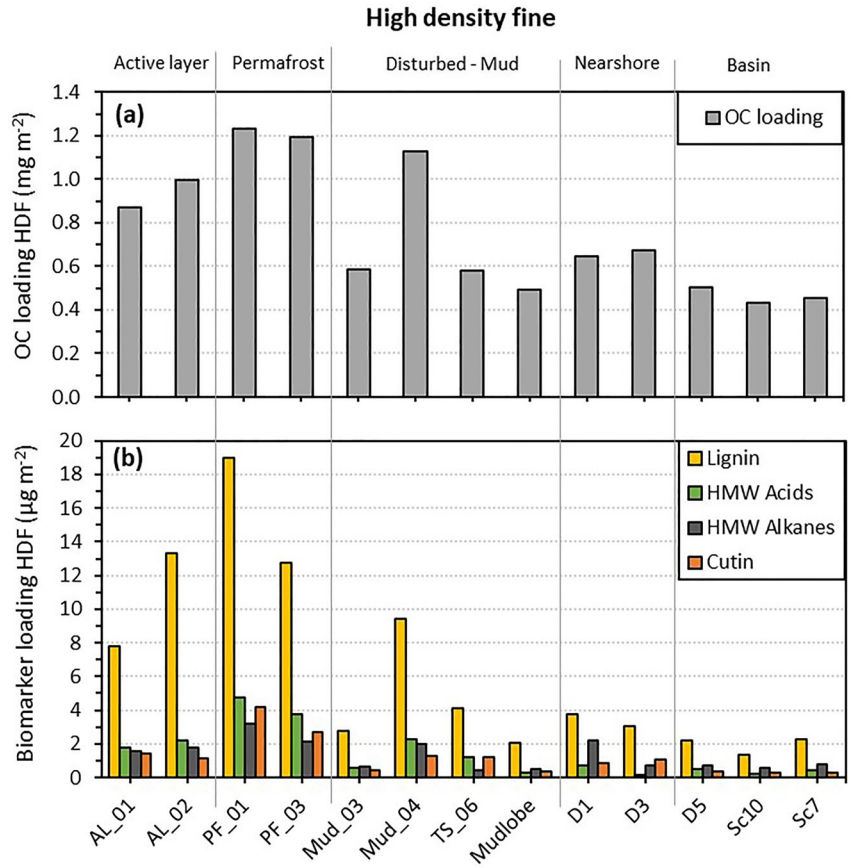

Figure 5. (a) Organic carbon (OC) loading (mg OC m^{-2}), and (b) biomarker loadings (µg biomarker m^{-2}) of lignin, HMW *n*-alkanoic acids, HMW *n*-alkanes and cutin of the high density fine (>1.8 g cm^{-3}, <63 µm) fraction of land, nearshore and basin sediments across the transect from land to ocean.

2.6. Molecular Geochemical Analyses

2.6.1. CuO-Oxidation Products: Lignin and Cutin

Microwave-assisted alkaline CuO oxidation was performed for the extraction of lignin and cutin products from both the HDF and the LD fractions, following Goñi and Montgomery (2000). Teflon extraction vessels were loaded with 2–4 mg OC, 500 mg CuO and 50 mg ferrous ammonium sulfate and 10 mL of degassed 2 N NaOH solution were added under oxygen-free conditions. The oxidation was performed in a MARS 6 microwave (CEM Cooperation) at 150°C (1,600 W, 8 min ramp, continued heating for 90 min). The resulting extract was centrifuged, transferred to glass vials, and spiked with an internal recovery standard (Ethyl vanillin; Sigma-Aldrich). The samples were acidified to pH 1 by adding concentrated HCl (37%), and extracted twice with ethyl acetate. The samples were dehydrated with anhydrous sodium sulfate, transferred to clean amber glass vials, and dried under N_2. Samples were re-dissolved in pyridine and methylated with BSTFA (N,O-Bis(trimethylsilyl)trifluoroacetamide) before analyses on an Agilent gas chromatograph-mass spectrometer (GC-MS) at the National Research Council Institute of Polar Sciences (Bologna, Italy). Quantification of individual lignin phenols, benzoic acids, and *p*-hydroxybenzenes was done using commercially available standards, and quantification of cutin-derived products was done using the response of trans-cinnamic acid.

The lignin content, either normalized to OC (mg g^{-1} OC), or mineral SA (µg m^{-2}), refers to the sum of vanillyl (V), syringyl (S) and cinnamyl (C) phenols, which is an indicator for the contribution of higher/vascular plant material to the total OM pool. These lignin-derived phenols have been extensively used to characterize and trace different pools of OC on land, in rivers and in the marine environment (e.g., Amon et al., 2012; Louchouarn et al., 2000; Salvadó et al., 2016; Tesi et al., 2014). The ratios between these lignin phenol

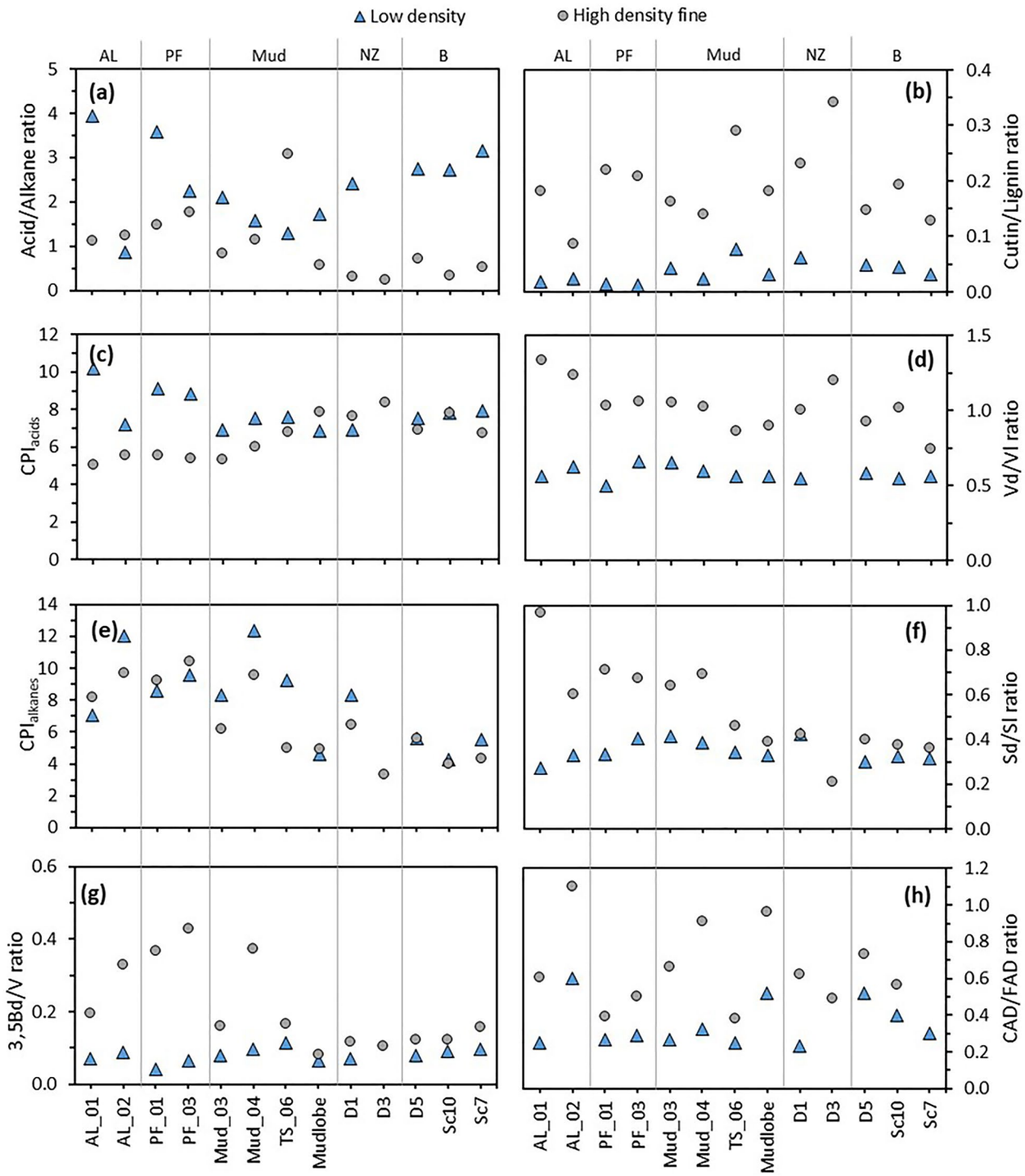

Figure 6. Comparison of different biomarker ratios of the high density fine (>1.8 g cm^{-3}, <63 μm) and the low density (<1.8 g cm^{-3}) fractions of land, nearshore and basin sediments across the transect from land to ocean. (a) Ratio between HMW *n*-alkanes and HMW *n*-alkanoic acids, (b) ratio between cutin and lignin, (c) the carbon preference index (CPI) of HMW *n*-alkanoic acids (CPI_{acids}), (d) ratio between Vd and Vl, (e) CPI of HMW *n*-alkanes ($CPI_{alkanes}$), (f) ratio between Sd and Sl, (g) ratio between 3,5Bd and V, (h) ratio between p-coumaric acid to ferulic acid (CAD/FAD).

groups (S/V and C/V) can be used to assess the various types of plants generating these phenols (Goñi & Hedges, 1992; Goñi & Montgomery, 2000; Hedges & Mann, 1979). Similarly, the cutin content refers to the sum of cutin-derived hydroxy fatty acids, which is a component of the leaves and needles of vascular plans (Goñi & Hedges, 1990).

The relative abundance of specific lignin phenol compound classes can also be used as indication for the degradation of OC. For instance, the acid/aldehyde ratio of vanillyl (Vd/Vl) and syringyl (Sd/Sl) phenols are often used as indicator for degradation of plant OM (Hedges et al., 1988; Opsahl & Benner, 1995). The aldehydes degrade faster than the corresponding acids, meaning that a higher Vd/Vl or Sd/Sl ratio points to more degraded material. Another CuO-oxidation products that is frequently used as degradation indicator is 3,5-Dihydroxybenzoic acid (3,5Bd), due to the recalcitrant nature of 3,5Bd, the ratio 3,5Bd/V increases with OC degradation in soils and sediments (Houel et al., 2006). Ratios of p-coumaric acid to ferulic acid (CAD/FAD) have also been used as an indicator for degradation in sediments and riverine dissolved organic carbon (DOC) (Amon et al., 2012; Houel et al., 2006) due to preferential degradation of ferulic acid and higher solubility of p-coumaric acid (Sanger et al., 1997).

2.6.2. Lipid Biomarkers

For lipid biomarker extraction, an amount of sediment containing 10–20 mg of OC was solvent-extracted twice with 15 mL dichloromethane:methanol (DCM:MeOH; 9:1 v/v) at 100°C (1,600 W, 5 min ramp, continued heating for 15 min), using a MARS 6 microwave (CEM Cooperation). The resulting extract was saponified with 10–15 mL of potassium hydroxide (KOH) in methanol (0.5 M) at 70°C for 2 hr. Subsequently, 5–10 mL of MilliQ water with 2% NaCl was added. The neutral fraction was extracted with hexane (3 × 10 mL), after which the samples were acidified to pH 2 with HCl (37%). The acid fraction was then extracted with hexane:DCM (4:1 v/v), methylated with BF_3-MeOH (80°C, 30 min), and extracted with DCM after the addition of MilliQ water.

The neutral fraction was further separated into an a-polar and polar fraction using silica column chromatrography (SiO_2, 5% water-deactivated), eluting first with hexane:DCM (9:1) for the a-polar fraction containing the *n*-alkanes, and then DMC:MeOH (1:1) for the polar fraction. The acid fraction was further cleaned of impurities using the same silica column chromatography setup, eluting first with hexane, then DCM:hexane (4:1), and finally DCM.

The a-polar neutral fraction and the cleaned methylated *n*-alkanoic acids, concentrated in the DCM:hexane fraction, were then analyzed on a GC-MS at the National Research Council Institute of Polar Sciences (Bologna, Italy). Quantification of high molecular weight (HMW; i.e., Carbon chain length n = 24–30) n-alkanes and n-alkanoic acids was done by comparison with commercially available standards (Sigma-Aldrich).

The carbon preference index (CPI) of these HMW *n*-alkanes and *n*-alkanioc acids is calculated as the ratio between odd and even carbon chain lengths (Equation 1 for alkanes, Equation 2 for acids). The CPI is indicative of OM maturity, since fresh plant material has a strong odd-over-even preference for *n*-alkanes, and even-over-odd for *n*-alkanoic acids (Eglinton & Hamilton, 1967; Freeman & Pancost, 2014), OM with lower CPI values is generally more degraded.

$$\mathrm{CPIalkanes} = \frac{\left(\frac{1}{2} * [C23 + C25 + C27 + C29 + C31]\right)}{[C22 + C24 + C26 + C28 + C30]} + \frac{\left(\frac{1}{2} * [C23 + C25 + C27 + C29 + C31]\right)}{[C24 + C26 + C28 + C30 + C32]} \quad (1)$$

$$\mathrm{CPIacids} = \frac{\left(\frac{1}{2} * [C24 + C26 + C28 + C30]\right)}{[C23 + C25 + C27 + C29]} + \frac{\left(\frac{1}{2} * [C24 + C26 + C28 + C30]\right)}{[C25 + C27 + C29 + C31]} \quad (2)$$

3. Results

3.1. Weight- and Organic Carbon Partitioning

The partitioning of the three sediment fractions is considerably different between samples from land, nearshore and basin (Figure 3a). In general, the HDF fraction is (in weight) dominant in samples from land (average 70%) and in the basin (more than 90%), while the HDC fraction is highest in the two samples in the nearshore zone (42.1% and 91.1%). The LD fraction contributes least to the total weight, ranging from 2.8% to 14.8% on land, and <2% for the marine samples. Notable outliers are sample TS_06, which is a sample of particulate matter in suspension in a TS and hardly contains HDC material, and sample D3, sampled in the shallow nearshore zone, which hardly contained LD material. Total mass recoveries of the fractionation method are between 81.9% and 96.5%, with a mean of 92.1 ± 3.5%, which is consistent with previous fractionation studies (Schreiner et al., 2013, 2014; Tesi et al., 2016; Wakeham et al., 2009). Data are presented in Figure 3a as percentage of the total recovered weight.

Total OC concentrations vary widely between the three fractions and between terrestrial and marine samples. The LD fraction is by far the most OC-rich, with a mean OC content of 21.8 ± 5.3%, while the HDC and HDF fractions contain 1.2 ± 1.0% and 1.9 ± 1.1% OC, respectively (Figure 4). Furthermore, the HDC and HDF fractions are richer in OC and more variable in the permafrost, AL and mud samples (1.6 ± 1.1% HDC and 2.5 ± 1.0% HDF, respectively) than in marine sediment (0.5 ± 0.3% and 0.8 ± 0.1%, respectively).

In the partitioning of OC (Figure 3b), the LD fraction (being OC-rich) plays a larger role than for sediment weight, contributing between 7.2%—59.6% (mean of 29.6%) to the bulk OC. The opposite is true for the HDC fraction, which contributes more to weight and less to TOC (0.1%–60%, mean of 12.5%). With only three exceptions (Mud_04, D1 and D3), most of the OC resides in the HDF fraction (32.7%–78.3%, mean of 57.9%).

3.2. Elemental Ratios and Carbon Isotopes

In the LD fraction, we find high C/N ratios of 18.7–28.2 (Figure 4b), with no apparent trend along the transect or difference between terrestrial and marine samples. For the HDF fraction, we find much lower values of 10.3–15.0, with a slight trend toward lower values moving from land to basin. The HDC fraction C/N values lie between the values of LD and HDF for all samples.

A very narrow range of $\delta^{13}C$ values is found in all samples and all fractions of this study, between −27.0‰ and −25.6‰ VPDB, with no significant differences between fractions nor between terrestrial and marine samples.

For $\Delta^{14}C$ (Figure 4c), the lowest values (i.e., oldest OC) are found in the HDF fraction of the disturbed zone samples (−537 to −918‰; corresponding to 6,500 to 20,000 ^{14}C years) and marine sediment samples (−789 to −840‰; 12,400 to 14,700 ^{14}C years) and, interestingly, not in permafrost samples (−402 and −537‰; 4,100 and 6,100 ^{14}C years). As expected, the AL samples showed the highest $\Delta^{14}C$ values (i.e., youngest OC) of all HDF fractions, of −334 and −338‰ (about 3,200 ^{14}C years).

The LD fraction showed consistently higher $\Delta^{14}C$ values than the HDF fraction (−123 to −826‰, 1,000 to 14,000 ^{14}C years), with the LD fraction being on average 2,800 ^{14}C years younger than the HDF fraction. The AL samples show again the highest $\Delta^{14}C$, at −123 and −155‰ (1,000 and 1,300 ^{14}C years), and the marine sediment samples the lowest, at −538 to −809‰ (6,100 to 14,000 ^{14}C years). The HDC fraction displayed values close to either the HDF or LD fraction (Figure 4c), except the three "basin" samples, which were younger than both of the other fractions.

3.3. Mineral Surface Area and Organic Carbon Loading

The mineral SA of the HDF fraction was measured to determine the available SA for mineral-bound carbon. It decreases along the transect, from 35 $m^2\ g^{-1}$ in the AL and 29 $m^2\ g^{-1}$ in permafrost, to 21–25 $m^2\ g^{-1}$ in mud, and 10–13 $m^2\ g^{-1}$ in nearshore marine sediments, followed by an increase in basin sediments to 17–21 $m^2\ g^{-1}$.

The concentration of OC normalized to mineral SA, or OC loading (in mg OC m^{-2}), can be used as a measure for the amount of mineral-bound OC in the sediment. Fine-grained sediment has a high SA available for mineral-bound carbon, and due to the loose organic debris being separated out through the density fractionation step, it can be assumed that nearly all OC in the HDF fraction is mineral-bound (Tesi et al., 2016). A clear ∼50% decrease can be seen in OC loading in the HDF fraction along the transect, from 0.9—1.2 mg OC m^{-2} in undisturbed terrestrial samples to 0.4–0.5 mg OC m^{-2} in basin sediments (Figure 5a). This trend in OC loading correlates well with the decrease in C/N ratio (Figure 7a; $R^2 = 0.84$, $p < 0.01$).

3.4. Biomarker Concentrations and Loading

The OC-normalized concentrations of four terrigenous biomarkers (HMW *n*-alkanes, HMW *n*-alkanoic acids, lignin phenols and cutin acids) of the LD and HDF fraction show that lignin is the most abundant biomarker in both the LD and HDF fraction (58.7–9.3 mg g^{-1} OC for LD and 17.9–3.1 mg g^{-1} OC for HDF). While lignin concentrations are higher in the LD fraction than in the HDF fraction, cutin and HMW *n*-alkanes concentrations are higher in HDF fraction (3.9–0.6 mg g^{-1} OC and 3.4–0.7 mg g^{-1} OC, respectively) than in the LD fraction (1.5–0.4 mg g^{-1} OC and 1.8–0.6 mg g^{-1} OC, respectively). The HMW *n*-alkanoic acids in the LD fraction

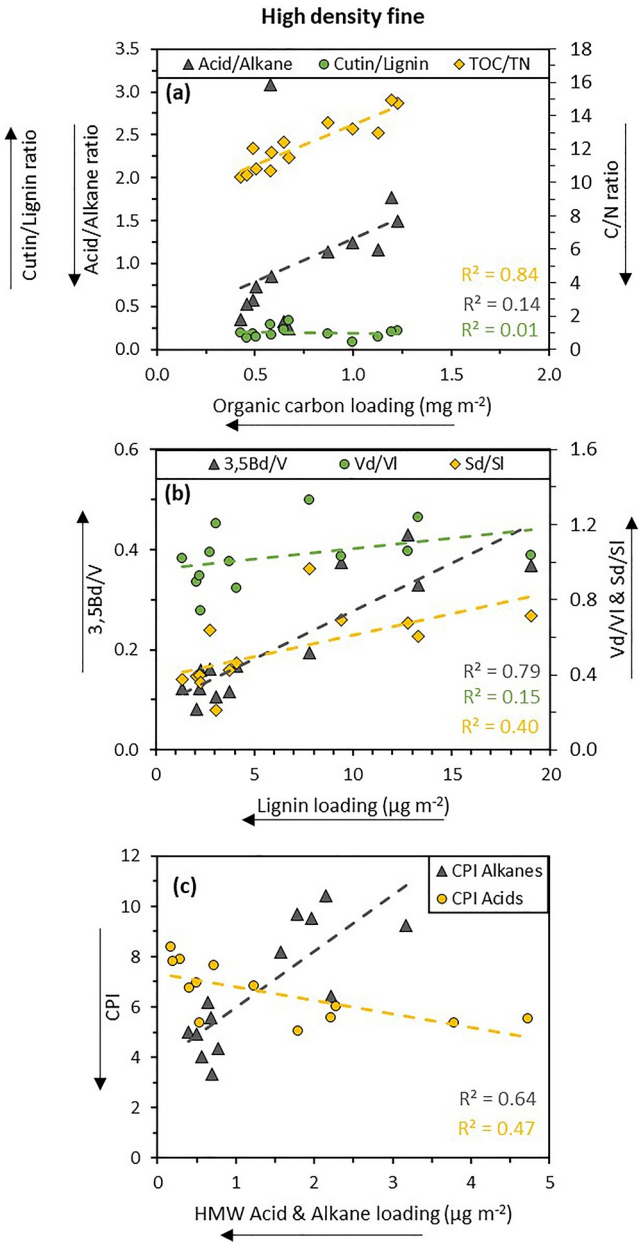

Figure 7. Correlations between organic carbon (OC) and biomarker loading (mg OC or µg biomarker per m^2) and degradation proxies of the high density fine sediment fraction (>1.8 g cm^{-3}, <63 µm) for (a) the C/N, cutin/lignin and acid/alkane ratio versus the total organic carbon loading (b) the CuO-oxidation product ratios (3,5Bd/V, Vd/Vl and Sd/Sl) versus the total lignin loading, and (c) the carbon preference index of HMW *n*-alkanoic acids (CPI_{acids}) and HMW *n*-alkanes ($CPI_{alkanes}$) versus their respective loading. The arrows next to the vertical axes represent loss of OC based on commonly used proxies for degradation of organic matter (OM) in soils and sediments, pointing in the direction of more degraded OM. The arrows next to the horizontal axes represent actual loss of OM from this sediment fraction.

showed rather consistent values along the transect (between 2.6—0.6 mg g^{-1} OC), while the HMW *n*-alkanoic acid concentrations in the HDF fraction decreased from terrestrial samples (4.5–0.9 mg g^{-1} OC) to marine samples (1.1–0.3 mg g^{-1} OC).

Note that for one sample (D3_LD) we were not able to extract enough material for accurate quantification of biomarkers. In summary, cutin acids and HMW *n*-alkanes are more abundant in the HDF fraction, while lignin phenols and HMW *n*-alkanoic acids are more abundant in the LD fraction, which is reflected in the cutin to lignin ratios (consistently higher for the HDF fraction) and the acid to alkane ratios (generally higher for the LD fraction) of the samples (Figures 5a and 5b).

The SA-normalized loadings of the terrestrial biomarkers of the HDF fraction (as µg m^{-2}) show that the permafrost samples have the highest loadings for all four measured biomarkers, followed by the AL and mud samples (Figure 5). The basin samples, on the contrary, show the overall lowest biomarker loading. The decreasing trend seen in the loadings of each of the biomarker groups matches the decrease seen in total OC loading of the HDF fraction (Figure 5; $p < 0.01$) However, the biomarker loadings show an overall stronger (~70–90%) decrease than the OC loading (~50%), when comparing the "undisturbed" AL and PF samples to the marine basin samples.

3.5. Biomarker Proxies for Organic Matter Degradation

In our terrestrial samples both the Sd/Sl and the Vd/Vl ratio of the HDF fraction are significantly higher (Sd/Sl 0.21–0.97, mean 0.53; Vd/Vl 0.74–1.33, mean 1.03) than the LD fraction (Sd/Sl 0.27–0.42, mean 0.35; Vd/Vl 0.50–0.66, mean 0.58) (Figures 6d and 6f). In the marine samples, the Vd/Vl of the HDF fraction remains considerably higher, while the Sd/Sl of the HDF fraction is only slightly higher than the LD fraction (Figures 6d and 6f). The 3,5Bd/V ratio of the LD fraction shows low values across the entire transect, between 0.04 and 0.12, and no trend moving from the terrestrial part to the basin (Figure 6g). In contrast, the 3,5Bd/V ratio of the HDF fraction does show a difference between the terrestrial samples (0.08–0.38) and the marine samples (0.11–0.16), though values are still consistently higher than the LD fraction (Figure 6g). The CAD/FAD ratio shows consistently higher values for HDF than for LD, but no trend over the transect (Figure 6h). Note that the CAD concentration for sample Sc7 was too close to the background value, so a ratio could not reliably be calculated for this sample.

The $CPI_{alkanes}$ slightly decreases along the transect for both the LD and HDF fraction, with higher values for the four "undisturbed" AL and permafrost (PF) samples (7.0–12.0) and lower values for the five marine samples (3.3–8.3). The $CPI_{alkanes}$ values are in the same range for both the LD and the HDF fraction (4.3–12.4 and 3.3–10.4 respectively) (Figure 6e). In contrast, the CPI_{acids} values shows a difference between the LD and the HDF fraction; while the LD fraction has a slightly higher CPI_{acids} for the PF and AL samples (7.2–10.2) compared to the marine samples (6.8–7.9), the CPI_{acids} of the HDF fraction steadily increases across the transect, from 5.0—5.6 for AL and PF toward 6.8–8.4 for the marine samples (Figure 6c).

It can be seen that the 3,5Bd/V ratio shows a strong positive correlation to lignin loading (Figure 7b; $R^2 = 0.79$, $p < 0.01$) and the $CPI_{alkanes}$ shows a positive correlation to the alkane loadings (Figure 7c; $R^2 = 0.64$, $p < 0.01$) when comparing these degradation proxies to the surface-area normalized biomarker concentrations of the HDF fraction. The Sd/Sl and

Vd/Vl however show no significant correlation to lignin biomarker loading (Figure 7b; $R^2 = 0.40$, $p = 0.02$ and $R^2 = 0.15$, $p = 0.19$, respectively), and CPI_{acids} even shows a weak negative relation to the acid loadings (Figure 7c; $R^2 = 0.47$, $p < 0.01$).

4. Discussion

4.1. Spatial OC Distribution and Hydrodynamic Sorting Along the Land-To-Ocean Transect

It is known that soil and sediment consist of a mix of mineral and organic components, with distinctive physical properties. These physical properties determine the OC content, its transport pathway and fate during transport. Soil/sediment OC can either be attached to mineral particles (mineral-bound OC) or not (matrix-free organic debris), and the size and density of these particles affects the behavior in the marine system, due to the differences in settling velocity and hydrodynamic sorting of sediment and its associated OC during aquatic transport (Ausín et al., 2021; Bao et al., 2018; Höfle et al., 2013; Tesi et al., 2016). This makes comparing bulk sediment samples from different energetic environments difficult, and may prove to be insufficient to fully resolve the fate of terrestrial OC. Due to sorting and winnowing a specific fraction of sediment may be absent or over-represented in a bulk sample, and thereby skewing OC content (Ausín et al., 2021; Radosavljevic et al., 2022). Our results show that OC concentrations vary significantly between fractions, .e. the LD fraction contains up to 10x more OC (21.8 ± 5.3%) than the HDF and HDC fractions (1.9 ± 1.1% and 1.2 ± 1.0% respectively). This LD fraction thus plays a larger role in the transport of OC than initially expected based on its contribution to the overall sediment by mass alone. Similar OC partitioning patterns were seen in earlier sediment and soil fractionation studies, for example, Tesi et al. (2016) found an OC% of marine sediment LD fraction of 18.2%–35.4% in the LD fraction of marine system, representing ~35–45% of the total OC in coastal bulk sediments.

We found a substantial difference in the partitioning of the three OC fractions traveling through different energetic "zones"; from a medium-energy "disturbed zone," via a high-energy nearshore zone, to a low-energy depositional area in an enclosed basin offshore (Tanski et al., 2017; Jong et al., 2020: for the definition of these zones). While the undisturbed zones on land (AL and PF) and in the basin appear relatively constant in OC partitioning, keeping the limited sample size in mind, the "disturbed zone" and the "nearshore zone" show a wide variation in partitioning. The trend in partitioning along the pathway of transport is as follows: the HDF fraction—mineral bound carbon—is transported farthest away, with the largest part of it ending up in the basin; the HDC fraction remains relatively close to shore in the high-energy nearshore zone, where the fine material is winnowed out by wave action, and the LD fraction—matrix-free organic debris—appears, somewhat surprisingly, most prominent in the disturbed zone and the shallow nearshore zone, likely due to the large size of particles in this fraction, causing them to settle rapidly (Bianchi et al., 2002; Goñi et al., 1998; Tesi et al., 2016; Wakeham et al., 2009).

In the shallow nearshore zone at 0.6 m water depth (sample D1) most OC is found in the LD fraction. While this sample did contain a large fraction of >1 mm organic particles that would settle rapidly, it is also likely that temporary accumulation happens in the very shallow part of the nearshore zone during fair weather, containing LD material that would otherwise be resuspended and washed away by wave action. In deeper waters, at 4.8 m water depth (sample D3), it is notable that most of the OC is located in the HDC fraction instead of the LD material, likely contained in black particles that were observed in the HDC fraction of sample D3 consisting of organic debris that is dense and coarse enough to end up in this fraction. In the basin most OC resides in the HDF fraction, but still >20% of OC is present in the LD fraction. The LD fraction of the basin samples consisted mostly of a fine, black powder, and contained less coarse particles. Our results show sharp differences in OC distribution among different hydrodynamic zones on the transect from land to basin, and a high variability of OC concentration comparing the three different hydrodynamic sediment fractions.

4.2. Contrasting Chemical Composition of the Different Size- and Density Fractions

Next to the high variability in OC concentration, the different sediment fractions of this study show distinct OM compositions. The LD fraction shows a C/N ratio consistent with fresh vegetation OM across the transect from land to basin, correspondingly low cutin/lignin ratios and high acid/alkanes ratios. In contrast, the HDF fraction shows low C/N ratios, with a decreasing trend from land to ocean. The lower C/N ratio of HDF on land is consistent with soil OM, but for the marine part of the transect marine primary production (with low C/N ratios) may also play a role. However, since the $\delta^{13}C$ does not show much variability and any marine algae present in the

sediment would likely end up in the LD fraction, the influence of marine primary production on the C/N ratio of the HDF fraction is considered to be negligible. Previous studies have shown that over 90% of OC present in Herschel Basin sediments is derived from terrestrial sources (Couture et al., 2018; Grotheer et al., 2020). The cutin/lignin ratios of the HDF fraction is consistently higher than the LD fraction, and the acid to alkane ratios lower (Figure 6b). These findings suggest that the LD fraction consist mostly of terrestrial matrix-free plant OM, and the HDF fraction consist mostly of terrestrial mineral-bound soil OM, which is in line with earlier sediment fractionation studies (Höfle et al., 2013; Tesi et al., 2016; Wakeham et al., 2009).

Furthermore, our results show that the age of the OC in the LD fraction is consistently younger than the HDF fraction (Figure 4c), which corroborates the finding that the LD fraction is relatively fresh, matrix-free organic debris. In contrast, the HDF fraction appears more aged, mineral-bound soil OM. Note that the ^{14}C age of our sampled permafrost was younger than any of the disturbed and marine fractions. This can be explained by the fact that the samples were collected from the Holocene-aged permafrost layer ("Unit 3"; Fritz et al., 2012), and not the Pleistocene permafrost ("Unit 2"; Fritz et al., 2012) that is much older. Most of the subsurface of Herschel Island—*Qikiqtaruk* consists of Pleistocene deposits (^{14}C age of 13,000–51,000 years; Fritz et al., 2012; Grotheer et al., 2020), which explains why the ^{14}C ages in disturbed and marine samples are higher than would have been expected based on our Holocene permafrost ages. Apart from the age difference between the sampled Holocene permafrost and the Pleistocene permafrost, the TOC%, $\delta^{13}C$, C/N ratio, and grain size distribution of the two permafrost units are similar on Herschel Island—*Qikiqtaruk* (Fritz et al., 2012), so that the permafrost age sampling bias should not affect the bulk OM results.

The difference between the HDF and LD fraction is consistent along the entire transect, and seems relatively unaffected by mixing of material from diverse sources in the disturbed and the nearshore zone. These two fractions contain distinctly different OC pools—relatively fresh vegetation (LD) versus reworked soil OC (HDF), and the combination of these disparate chemical and physical characteristics influence the distribution of OC and the signature of the "bulk" sediment OC. Measuring only bulk sediment will not provide sufficient information to disentangle the transport pathway of these specific hydrodynamic fractions across dynamic sedimentary environments, or when comparing terrestrial and marine samples to each other.

4.3. Substantial Loss of Terrestrial OC From Mineral Particles (HDF) After Mobilization and Transport

The change in OC content per square meter of mineral SA (OC "loading") can be used to quantitatively assess loss of OC from sediment due to degradation and/or desorption (Aller & Blair, 2006; Freymond et al., 2018; Keil et al., 1994). A drawback of this method is the assumption that all the OC is associated with the mineral matrix, which can be skewed by loose organic debris or OC-free sand particles (Tesi et al., 2016). Since we isolated loose organic debris (i.e., the LD fraction) and OC-free sand particles (i.e., HDC) from the fraction where OC is mostly associated with the mineral matrix (i.e., the HDF), we can reliably normalize to mineral SA and compare samples along a transect across different sedimentary environments.

A strong decrease of the OC- and terrestrial biomarker loading was found in the HDF fraction, with a loss of ∼50% of OC and ∼70–90% of the biomarkers along the transect that crosses the land-ocean boundary (Figure 5). This is consistent with previous studies that show bulk or molecular loss of terrestrial OC along various transects on either side of the land-ocean boundary for example, in the East Siberian Sea (Alling et al., 2010; Karlsson et al., 2016; Tesi et al., 2014), or the Peel River (Bröder et al., 2021; Keskitalo et al., 2021) and on land on Herschel Island—*Qikiqtaruk* (Tanski et al., 2017). "Loss" of OC can mean degradation of OC bound to the mineral particles, and/or desorption of bound OC into suspended (POC) or DOC pools. While literature shows that DOC degrades rapidly in the water column (Abbott et al., 2014; Mann et al., 2012; Vonk et al., 2013), POC is found to be rapidly redeposited (e.g., Jong et al., 2020). Offshore transport of POC along the seabed or in the nepheloid layer continues to expose POC to degradation over long timescales. Prior to entry into the marine system, loss of OC is likely already occurring on land via freeze-thaw cycling, deposition-remobilization processes and leaching (Tanski et al., 2017) and in the nearshore zone via resuspension, winnowing, and wave/storm action (Grotheer et al., 2020; Jong et al., 2020).

While mineral-bound OC has been found to be relatively "protected" against microbial degradation (Keil et al., 1994), mineral protection of OC does not hold in all conditions, and should be considered as a multidimensional and multifaceted component of the cycling of OC (Kleber et al., 2021). Processes such as adsorption

and desorption of OC take place during transport and after deposition of sediment, affecting the state of mineral bound-OC on its path from source to sink. We observe a significant loss of OC in the HDF fraction over only a short distance (5 km), indicating loss of mineral-bound OC. We want to highlight that this short transect includes both terrestrial and marine settings and also includes very dynamic and energetic environments, where materials cross the frozen-thawed, as well as the freshwater-saltwater interface. These dynamic transitional zones appear to play a crucial role in processing terrestrial OC.

4.4. Biomarker Proxies Show Contrasting Patterns

On a molecular level, a large contrast can be seen comparing the LD and the HDF fraction. In general, the LD fraction appears "fresher" than the HDF fraction with Vd/Vl and CAD/FAD ratios showing overall more degraded values for the HDF fraction and "fresher" values for the LD fraction (Figures 6d and 6h). The CPI_{acids}, Sd/Sl and the 3,5Bd/V ratios show that the HDF fraction is much more degraded than the LD fraction in the AL and PF, which appears to even out in the marine samples (Figures 6c, 6f, and 6g). In contrast, the $CPI_{alkanes}$ shows no significant difference between the LD and HDF fraction (Figure 6e). The molecular distinction in degradation status of the LD and HDF fractions confirms the earlier observations based on C/N, acids/alkanes, and cutin/lignin (Section 4.2) suggesting that the LD fraction is comprised of relatively fresh, loose organic debris and the HDF fraction of more reworked, mineral-bound OC.

However, the contrasting patterns comparing terrestrial and marine samples are surprising. While we would expect a quantitative loss of OC (decrease in mineral-bound OC and mineral-bound biomarkers) to be coupled with an overall qualitative change of the remaining OM (seen in biomarker proxies) with ongoing degradation along a transport pathway of OC, we find contrasting patterns and ambiguity instead. Following the results discussed in Section 4.3, we would have expected that biomarker degradation proxies in the HDF fraction show a similar, consistent trend of fresh material on land versus more degraded material in the marine setting. Instead, we find contrasting trends along the transect and with OC loading (Figures 5 and 7). Only one proxy, the $CPI_{alkanes}$, indicates more degraded OC with increasing distance from the "source" of the OC, and shows a positive correlation to the HMW *n*-alkane loading. However, lower $CPI_{alkanes}$ in the basin could also indicate a contribution of petrogenic-derived material known to be present in the Mackenzie river system nearby (Behnke et al., 2023; Bröder et al., 2021; Goñi et al., 2005; Yunker et al., 1993). Despite Herschel Basin being semi-enclosed, where bulk of the material comes from regional sources, some influence from the Mackenzie river persists and input of material from a petrogenic origin cannot be excluded (Bröder et al., 2021; Goñi et al., 2005; Grotheer et al., 2020; Yunker et al., 1993). The other proxies show the opposite (CPI_{acids} and 3,5Bd/V), that is, a fresher signature toward the basin, or no trend at all (Vd/Vl). For the LD fraction, only $CPI_{alkanes}$ shows a clear pattern along the transect, with a trend suggesting degradation of OM moving from land to the basin, or, same as for the HDF fraction, a contribution of petrogenic origin.

Comparable ambiguities in terrestrial biomarker degradation proxies were also found in other recent studies (i.e., Bröder et al., 2021; Tanski et al., 2021; Tesi et al., 2016). The 3,5Bd/V ratio in Tesi et al. (2016) shows a steady increase in this ratio in all sediment fractions across a (up to) 600 km transect across the East Siberian- and Laptev Sea in contrast to our—overall—decreasing values. However, within our marine sediment samples only (D1—Sc7, a 5 km transect), a slight positive trend can be seen in 3,5Bd/V in both the HDF and LD fraction moving offshore (Figure 6g), which could indicate that this ratio works as a degradation proxy in relatively static or homogeneous settings, and not in dynamic transition zones such as the nearshore zone or other land-ocean transition zones. Alternatively, lignin-based proxies could require longer transport time and degradation extent to produce a measurable change in the biomarker fingerprint as opposed to the loading of terrestrial carbon that exhibited a rather large change over a relatively short distance (Goñi et al., 2000; Tesi et al., 2014). This would lead to the conclusion that some biomarker indices for degradation of OC may need revision and/or need to be used under specific circumstances only. By combining molecular biogeochemical proxies with sedimentological measurements and hydrodynamic sediment fractionation/separation, we can better identify which proxy works under which circumstances (e.g., spatially, temporally, or transition-zone specific), and more accurately quantify degradative loss of OC during transport.

5. Conclusion

Comparing permafrost-derived sediment OC within dynamic sedimentary environments is challenging. Transport, sorting and winnowing of sediment when moving through the nearshore zone to an offshore basin creates a

transition from coarse sediment nearshore, to fine sediment in the offshore basin. This affects the distribution of OC, which is part of the sediment, and can be bound to mineral particles. Fractionation of soils and sediments into low (LD, <1.8 g cm^{-3}) and a high-density fraction, and separating HD in fine (HDF, <63 μm) and coarse fractions (HDC, >63 μm) here shows a substantial contrast between different environments and comparing weight with OC partitioning. Biomarker analyses, C/N ratio and carbon isotopes show that the OC in the LD fraction is a younger, fresher, matrix-free OC pool, in contrast to the HDF fraction that appears more aged, mineral-bound soil OM.

Organic carbon and biomarker loading show that a significant amount of OC is lost from the HDF fraction through desorption and/or degradation of OC bound to fine sediments along a 5 km land—basin transect. We estimate that up to 50% of mineral-bound OC may be lost along this transect, while for specific terrestrial biomarkers this decrease can be even higher, up to 90%. While the transect is very short, it crosses multiple energetic and transitional environments along the land-ocean continuum (to our knowledge not done before), which can potentially explain the high OC losses. At the same time, molecular degradation proxies showed contrasting patterns across that same distance, suggesting that losses of OC are not always reflected in the degradation state or "relative freshness" of the OC.

We propose to further integrate sedimentology, fractionation methods, and organic geochemistry and aim for standardized methods to better quantify storage, degradation and loss of terrestrial OC, particularly targeting dynamic terrestrial-aquatic environments. Within more static environments such as deep ocean basins, bulk OC analyses may be representative, though we recommend continuing analysis of specific sedimentary hydrodynamic fractions and their geochemical signatures when studying spatial transects within land-ocean transition zones. This approach allows for incorporation of sorting processes that impact the distribution of OC, as well as its potential mineral stabilization. These things are important for understanding the impact of terrestrial OC in rapidly changing arctic coastal ecosystems, and also for quantifying the ultimate impact of thawed permafrost OC on our global climate.

Data Availability Statement

Data used in this study can be accessed at the open access data repository PANGAEA: https://doi.org/10.1594/PANGAEA.960026 (Jong et al., 2024).

Acknowledgments

We wish to acknowledge funding from the European Research Council (StG THAWSOME, 676982) and European Union's Horizon 2020 Research and Innovation Programme (Nunataryuk, Grant 773421). We wish to thank Konstantin Klein, Dyke Scheidemann, Kirsi Keskitalo and the rangers of Herschel Island Qikiqtaruk Territorial Park for their help in the field. Furthermore, we wish to express our thanks to the Yukon Territorial Government and Yukon Parks, and also acknowledge the logistical support of the Aurora Research Institute (ARI, Inuvik), members of the Laboratory for Ion Beam Physics, ETH Zurich, and members of the Vrije Universiteit Amsterdam sediment lab.

References

Abbott, B. W., Larouche, J. R., Jones, J. B., Bowden, W. B., & Balser, A. W. (2014). Elevated dissolved organic carbon biodegradability from thawing and collapsing permafrost. *Journal of Geophysical Research: Biogeosciences*, *119*(10), 2049–2063. https://doi.org/10.1002/2014JG002678

Aller, R. C., & Blair, N. E. (2006). Carbon remineralization in the Amazon-Guianas tropical mobile mudbelt: A sedimentary incinerator. *Continental Shelf Research*, *26*(17–18), 2241–2259. https://doi.org/10.1016/j.csr.2006.07.016

Alling, V., Sanchez-Garcia, L., Porcelli, D., Pugach, S., Vonk, J. E., Van Dongen, B., et al. (2010). Nonconservative behavior of dissolved organic carbon across the Laptev and East Siberian seas. *Global Biogeochemical Cycles*, *24*(4), 1–15. https://doi.org/10.1029/2010GB003834

Amon, R. M. W., Rinehart, A. J., Duan, S., Louchouarn, P., Prokushkin, A., Guggenberger, G., et al. (2012). Dissolved organic matter sources in large Arctic rivers. *Geochimica et Cosmochimica Acta*, *94*, 217–237. https://doi.org/10.1016/j.gca.2012.07.015

Ausín, B., Bruni, E., Haghipour, N., Welte, C., Bernasconi, S. M., & Eglinton, T. I. (2021). Controls on the abundance, provenance and age of organic carbon buried in continental margin sediments. *Earth and Planetary Science Letters*, *558*, 116759. https://doi.org/10.1016/j.epsl.2021.116759

Bao, R., Blattmann, T. M., McIntyre, C., Zhao, M., & Eglinton, T. I. (2019). Relationships between grain size and organic carbon 14C heterogeneity in continental margin sediments. *Earth and Planetary Science Letters*, *505*, 76–85. https://doi.org/10.1016/j.epsl.2018.10.013

Bao, R., Uchida, M., Zhao, M., Haghipour, N., Montlucon, D., McNichol, A., et al. (2018). Organic carbon aging during across-shelf transport. *Geophysical Research Letters*, *45*(16), 8425–8434. https://doi.org/10.1029/2018GL078904

Behnke, M. I., Tank, S. E., McClelland, J. W., Holmes, R. M., Haghipour, N., Eglinton, T. I., et al. (2023). Aquatic biomass is a major source to particulate organic matter export in large Arctic rivers. *Proceedings of the National Academy of Sciences*, *120*(12), 2017. https://doi.org/10.1073/pnas.2209883120

Bianchi, T. S., Mitra, S., & McKee, B. A. (2002). Sources of terrestrially-derived organic carbon in lower Mississippi River and Louisiana shelf sediments: Implications for differential sedimentation and transport at the coastal margin. *Marine Chemistry*, *77*(2–3), 211–223. https://doi.org/10.1016/S0304-4203(01)00088-3

Bröder, L., Andersson, A., Tesi, T., Semiletov, I., & Gustafsson, Ö. (2019). Quantifying degradative loss of terrigenous organic carbon in surface sediments across the Laptev and East Siberian Sea. *Global Biogeochemical Cycles*, *33*(1), 85–99. https://doi.org/10.1029/2018GB005967

Bröder, L., Keskitalo, K., Zolkos, S., Shakil, S., Tank, S. E., Kokelj, S. V., et al. (2021). Preferential export of permafrost-derived organic matter as retrogressive thaw slumping intensifies. *Environmental Research Letters*, *16*(5), 054059. https://doi.org/10.1088/1748-9326/abee4b

Brunauer, S., Emmett, P. H., & Teller, E. (1938). Adsorption of gases in multimolecular layers. *Journal of the American Chemical Society*, *60*(2), 309–319. https://doi.org/10.1021/ja01269a023

Coppola, L., Gustafsson, Ö., Andersson, P., Eglinton, T. I., Uchida, M., & Dickens, A. F. (2007). The importance of ultrafine particles as a control on the distribution of organic carbon in Washington Margin and Cascadia Basin sediments. *Chemical Geology*, *243*(1–2), 142–156. https://doi.org/10.1016/j.chemgeo.2007.05.020

Couture, N. J., Irrgang, A., Pollard, W., Lantuit, H., & Fritz, M. (2018). Coastal erosion of permafrost soils along the Yukon Coastal Plain and fluxes of organic carbon to the Canadian Beaufort Sea. *Journal of Geophysical Research: Biogeosciences*, *123*(2), 406–422. https://doi.org/10.1002/2017JG004166

Doxaran, D., Ehn, J., Bélanger, S., Matsuoka, A., Hooker, S., & Babin, M. (2012). Optical characterisation of suspended particles in the Mackenzie River plume (Canadian Arctic Ocean) and implications for ocean colour remote sensing. *Biogeosciences*, *9*(8), 3213–3229. https://doi.org/10.5194/bg-9-3213-2012

Eglinton, G., & Hamilton, R. J. (1967). Leaf epicuticular waxes. *Science*, *156*(3780), 1322–1335. https://doi.org/10.1126/science.156.3780.1322

Freeman, K. H., & Pancost, R. D. (2014). Biomarkers for terrestrial plants and climate. In *Treatise on geochemistry* (pp. 395–416). Elsevier. https://doi.org/10.1016/B978-0-08-095975-7.01028-7

Freymond, C. V., Kündig, N., Stark, C., Peterse, F., Buggle, B., Lupker, M., et al. (2018). Evolution of biomolecular loadings along a major river system. *Geochimica et Cosmochimica Acta*, *223*, 389–404. https://doi.org/10.1016/j.gca.2017.12.010

Fritz, M., Vonk, J. E., & Lantuit, H. (2017). Collapsing Arctic coastlines. *Nature Climate Change*, *7*(1), 6–7. https://doi.org/10.1038/nclimate3188

Fritz, M., Wetterich, S., Schirrmeister, L., Meyer, H., Lantuit, H., Preusser, F., & Pollard, W. H. (2012). Eastern Beringia and beyond: Late Wisconsinan and Holocene landscape dynamics along the Yukon Coastal Plain, Canada. *Palaeogeography, Palaeoclimatology, Palaeoecology*, *319–320*, 28–45. https://doi.org/10.1016/j.palaeo.2011.12.015

Goñi, M. A., & Hedges, J. I. (1990). Cutin-derived CuO reaction products from purified cuticles and tree leaves. *Geochimica et Cosmochimica Acta*, *54*(11), 3065–3072. https://doi.org/10.1016/0016-7037(90)90122-2

Goñi, M. A., & Hedges, J. I. (1992). Lignin Dimers – structures, distribution, and potential geochemical applications. *Geochimica et Cosmochimica Acta*, *56*(11), 4025–4043. https://doi.org/10.1016/0016-7037(92)90014-a

Goñi, M. A., & Montgomery, S. (2000). Alkaline CuO oxidation with a microwave digestion system: Lignin analyses of geochemical samples. *Analytical Chemistry*, *72*(14), 3116–3121. https://doi.org/10.1021/ac991316w

Goñi, M. A., Ruttenberg, K. C., & Eglinton, T. I. (1998). A reassessment of the sources and importance of land-derived organic matter in surface sediments from the Gulf of Mexico. *Geochimica et Cosmochimica Acta*, *62*(18), 3055–3075. https://doi.org/10.1016/S0016-7037(98)00217-8

Goñi, M. A., Yunker, M. B., MacDonald, R. W., & Eglinton, T. I. (2000). Distribution and sources of organic biomarkers in arctic sediments from the Mackenzie River and Beaufort Shelf. *Marine Chemistry*, *71*(1–2), 23–51. https://doi.org/10.1016/S0304-4203(00)00037-2

Goñi, M. A., Yunker, M. B., Macdonald, R. W., & Eglinton, T. I. (2005). The supply and preservation of ancient and modern components of organic carbon in the Canadian Beaufort Shelf of the Arctic Ocean. *Marine Chemistry*, *93*(1), 53–73. https://doi.org/10.1016/j.marchem.2004.08.001

Grotheer, H., Meyer, V., Riedel, T., Pfalz, G., Mathieu, L., Hefter, J., et al. (2020). Burial and origin of permafrost-derived carbon in the nearshore zone of the southern Canadian Beaufort Sea. *Geophysical Research Letters*, *47*(3). https://doi.org/10.1029/2019GL085897

Günther, F., Overduin, P. P., Yakshina, I. A., Opel, T., Baranskaya, A. V., & Grigoriev, M. N. (2015). Observing Muostakh disappear: Permafrost thaw subsidence and erosion of a ground-ice-rich Island in response to arctic summer warming and sea ice reduction. *The Cryosphere*, *9*(1), 151–178. https://doi.org/10.5194/tc-9-151-2015

Haghipour, N., Ausin, B., Usman, M. O., Ishikawa, N., Wacker, L., Welte, C., et al. (2018). Compound-specific radiocarbon analysis by elemental analyzer–accelerator mass spectrometry: Precision and limitations. *Analytical Chemistry*, *91*(3), 2042–2049. research-article. https://doi.org/10.1021/acs.analchem.8b04491

Harper, J. R. (1990). Morphology of the Canadian Beaufort Sea coast. *Marine Geology*, *91*(1–2), 75–91. https://doi.org/10.1016/0025-3227(90)90134-6

Hedges, J. I., Blanchette, R. A., Weliky, K., & Devol, A. H. (1988). Effects of fungal degradation on the CuO oxidation products of lignin: A controlled laboratory study. *Geochimica et Cosmochimica Acta*, *52*(11), 2717–2726. https://doi.org/10.1016/0016-7037(88)90040-3

Hedges, J. I., & Mann, D. C. (1979). The characterization of plant tissues by their lignin oxidation products. *Geochimica et Cosmochimica Acta*, *43*(11), 1803–1807. https://doi.org/10.1016/0016-7037(79)90028-0

Höfle, S., Rethemeyer, J., Mueller, C. W., & John, S. (2013). Organic matter composition and stabilization in a polygonal tundra soil of the Lena Delta. *Biogeosciences*, *10*(5), 3145–3158. https://doi.org/10.5194/bg-10-3145-2013

Houel, S., Louchouarn, P., Lucotte, M., Canuel, R., & Ghaleb, B. (2006). Translocation of soil organic matter following reservoir impoundment in boreal systems: Implications for in situ productivity. *Limnology & Oceanography*, *51*(3), 1497–1513. https://doi.org/10.4319/lo.2006.51.3.1497

Hugelius, G., Strauss, J., Zubrzycki, S., Harden, J. W., Schuur, E. A. G., Ping, C. L., et al. (2014). Estimated stocks of circumpolar permafrost carbon with quantified uncertainty ranges and identified data gaps. *Biogeosciences*, *11*(23), 6573–6593. https://doi.org/10.5194/bg-11-6573-2014

Intergovernmental Panel on Climate Change (IPCC). (2023). *Climate change 2021 – The physical science basis: Working group I contribution to the sixth assessment report of the intergovernmental panel on climate change*. Cambridge University Press. https://doi.org/10.1017/9781009157896

Irrgang, A. M., Lantuit, H., Manson, G. K., Günther, F., Grosse, G., & Overduin, P. P. (2018). Variability in rates of coastal change along the Yukon Coast, 1951 to 2015. *Journal of Geophysical Research: Earth Surface*, *123*(4), 779–800. https://doi.org/10.1002/2017JF004326

Jong, D., Bröder, L., Tanski, G., Fritz, M., Lantuit, H., Tesi, T., et al. (2020). Nearshore zone dynamics determine pathway of organic carbon from eroding permafrost coasts. *Geophysical Research Letters*, *47*(15). https://doi.org/10.1029/2020GL088561

Jong, D., Bröder, L., Tesi, T., Keskitalo, K. H., Zimov, N., Davydova, A., et al. (2023). Contrasts in dissolved, particulate, and sedimentary organic carbon from the Kolyma River to the East Siberian Shelf. *Biogeosciences*, *20*(1), 271–294. https://doi.org/10.5194/bg-20-271-2023

Jong, D., Bröder, L., Tesi, T., Tanski, G., Oudenhuijsen, M., Fritz, M., et al. (2024). Sedimentological and biogeochemical composition of fractionated permafrost- and sediment organic carbon of the nearshore zone of Herschel Island [Dataset]. PANGAEA. https://doi.org/10.1594/PANGAEA.960026

Karlsson, E., Gelting, J., Tesi, T., Dongen, B., Andersson, A., Semiletov, I., et al. (2016). (pp. 898–919). Different sources and degradation state of dissolved, particulate, and sedimentary organic matter along the Eurasian Arctic coastal margin. *Global Biogeochemical Cycles*. https://doi.org/10.1002/2015GB005307

Keil, R. G., Montluçon, D. B., Prahl, F. G., & Hedges, J. I. (1994). Sorptive preservation of labile organic matter in marine sediments. *Nature*, *370*(6490), 549–552. https://doi.org/10.1038/370549a0

Keskitalo, K. H., Bröder, L., Shakil, S., Zolkos, S., Tank, S. E., van Dongen, B. E., et al. (2021). Downstream evolution of particulate organic matter composition from permafrost thaw slumps. *Frontiers in Earth Science*, *9*, 1–21. https://doi.org/10.3389/feart.2021.642675

Kleber, M., Bourg, I. C., Coward, E. K., Hansel, C. M., Myneni, S. C. B., & Nunan, N. (2021). Dynamic interactions at the mineral–organic matter interface. *Nature Reviews Earth & Environment*, *2*(6), 402–421. https://doi.org/10.1038/s43017-021-00162-y

Klein, K. P., Lantuit, H., Heim, B., Fell, F., Doxaran, D., & Irrgang, A. M. (2019). Long-term high-resolution sediment and sea surface temperature spatial patterns in arctic nearshore waters retrieved using 30-year landsat archive imagery. *Remote Sensing*, *11*(23), 2791. https://doi.org/10.3390/rs11232791

Komada, T., Anderson, M. R., & Dorfmeier, C. L. (2008). Carbonate removal from coastal sediments for the determination of organic carbon and its isotopic signatures, d13C and D14C: Comparison of fumigation and direct acidification by hydrochloric acid. *Limnology and Oceanography: Methods*, *6*, 254–262. https://doi.org/10.4319/lom.2008.6.254

Lantuit, H., Overduin, P. P., Couture, N., Wetterich, S., Aré, F., Atkinson, D., et al. (2012). The arctic coastal dynamics database: A new classification scheme and statistics on Arctic Permafrost Coastlines. *Estuaries and Coasts*, *35*(2), 383–400. https://doi.org/10.1007/s12237-010-9362-6

Louchouarn, P., Opsahl, S., & Benner, R. (2000). Isolation and quantification of dissolved lignin from natural waters using solid-phase extraction and GC/MS. *Analytical Chemistry*, *72*(13), 2780–2787. https://doi.org/10.1021/ac9912552

Macdonald, R. W., & Yu, Y. (2006). The Mackenzie estuary of the Arctic Ocean. In *Handbook of environmental chemistry, volume 5: Water pollution* (pp. 91–120). (PART H). https://doi.org/10.1007/698-5-027

Mann, P. J., Davydova, A., Zimov, N., Spencer, R. G. M., Davydov, S., Bulygina, E., et al. (2012). Controls on the composition and lability of dissolved organic matter in Siberia's Kolyma River basin. *Journal of Geophysical Research*, *117*(1), 1–15. https://doi.org/10.1029/2011JG001798

McIntyre, C. P., Wacker, L., Haghipour, N., Blattmann, T. M., Fahrni, S., Usman, M., et al. (2017). Online 13C and 14C gas measurements by EA-IRMS-AMS at ETH Zürich. *Radiocarbon*, *59*(3), 893–903. https://doi.org/10.1017/RDC.2016.68

Meyers, P. A. (1994). Preservation of elemental and isotopic source identification of sedimentary organic matter. *Chemical Geology*, *114*(3–4), 289–302. https://doi.org/10.1016/0009-2541(94)90059-0

Obu, J., Lantuit, H., Fritz, M., Pollard, W. H., Sachs, T., & Günther, F. (2016). Relation between planimetric and volumetric measurements of permafrost coast erosion: A case study from Herschel Island, western Canadian arctic. *Polar Research*, *35*, 1–13. https://doi.org/10.3402/polar.v35.30313

Obu, J., Lantuit, H., Grosse, G., Günther, F., Sachs, T., Helm, V., & Fritz, M. (2017). Coastal erosion and mass wasting along the Canadian Beaufort Sea based on annual airborne LiDAR elevation data. *Geomorphology*, *293*, 331–346. https://doi.org/10.1016/j.geomorph.2016.02.014

Opsahl, S., & Benner, R. (1995). Early diagenesis of vascular plant tissues: Lignin and cutin decomposition and biogeochemical implications. *Geochimica et Cosmochimica Acta*, *59*(23), 4889–4904. https://doi.org/10.1016/0016-7037(95)00348-7

Overeem, I., Anderson, R. S., Wobus, C. W., Clow, G. D., Urban, F. E., & Matell, N. (2011). Sea ice loss enhances wave action at the Arctic coast. *Geophysical Research Letters*, *38*(17), 1–6. https://doi.org/10.1029/2011GL048681

Radosavljevic, B., Lantuit, H., Knoblauch, C., Couture, N., Herzschuh, U., & Fritz, M. (2022). Arctic nearshore sediment dynamics—An example from Herschel Island—Qikiqtaruk, Canada. *Journal of Marine Science and Engineering*, *10*(11), 1589. https://doi.org/10.3390/jmse10111589

Rampton, V. N. (1982). Quaternary geology of the Yukon coastal plain.

Salvadó, J. A., Tesi, T., Sundbom, M., Karlsson, E., Krusä, M., Semiletov, I. P., et al. (2016). Contrasting composition of terrigenous organic matter in the dissolved, particulate and sedimentary organic carbon pools on the outer East Siberian Arctic Shelf. *Biogeosciences*, *13*(22), 6121–6138. https://doi.org/10.5194/bg-13-6121-2016

Sanger, L. J., Anderson, J. M., Little, D., & Bolger, T. (1997). Phenolic and carbohydrate signatures of organic matter in soils developed under grass and forest plantations following changes in land use. *European Journal of Soil Science*, *48*(2), 311–317. https://doi.org/10.1111/j.1365-2389.1997.tb00551.x

Schreiner, K. M., Bianchi, T. S., Eglinton, T. I., Allison, M. A., & Hanna, A. J. M. (2013). Sources of terrigenous inputs to surface sediments of the Colville River Delta and Simpson's Lagoon, Beaufort Sea, Alaska. *Journal of Geophysical Research: Biogeosciences*, *118*(2), 808–824. https://doi.org/10.1002/jgrg.20065

Schreiner, K. M., Bianchi, T. S., & Rosenheim, B. E. (2014). Evidence for permafrost thaw and transport from an Alaskan North Slope watershed. *Geophysical Research Letters*, *41*(9), 3117–3126. https://doi.org/10.1002/2014GL059514

Schuur, E. A. G., McGuire, A. D., Schädel, C., Grosse, G., Harden, J. W., Hayes, D. J., et al. (2015). Climate change and the permafrost carbon feedback. *Nature*, *520*(7546), 171–179. https://doi.org/10.1038/nature14338

Strauss, J., Schirrmeister, L., Mangelsdorf, K., Eichhorn, L., Wetterich, S., & Herzschuh, U. (2015). Organic-matter quality of deep permafrost carbon – A study from Arctic Siberia. *Biogeosciences*, *12*(7), 2227–2245. https://doi.org/10.5194/bg-12-2227-2015

Stuiver, M., & Polach, H. A. (1977). Discussion reporting of 14 C data. *Radiocarbon*, *19*(3), 355–363. https://doi.org/10.1017/S0033822200003672

Tanski, G., Bröder, L., Wagner, D., Knoblauch, C., Lantuit, H., Beer, C., et al. (2021). Permafrost carbon and CO2 pathways differ at contrasting coastal erosion sites in the Canadian Arctic. *Frontiers in Earth Science*, *9*, 630493. https://doi.org/10.3389/feart.2021.630493

Tanski, G., Lantuit, H., Ruttor, S., Knoblauch, C., Radosavljevic, B., Strauss, J., et al. (2017). Transformation of terrestrial organic matter along thermokarst-affected permafrost coasts in the Arctic. *Science of the Total Environment*, *581–582*, 434–447. https://doi.org/10.1016/j.scitotenv.2016.12.152

Tesi, T., Puig, P., Palanques, A., & Goñi, M. A. (2010). Lateral advection of organic matter in cascading-dominated submarine canyons. *Progress in Oceanography*, *84*(3–4), 185–203. https://doi.org/10.1016/j.pocean.2009.10.004

Tesi, T., Semiletov, I., Dudarev, O., Andersson, A., & Gustafsson, Ö. (2016). Matrix association effects on hydrodynamic sorting and degradation of terrestrial organic matter during cross-shelf transport in the Laptev and East Siberian shelf seas. *Journal of Geophysical Research: Biogeosciences*, *121*(3), 731–752. https://doi.org/10.1002/2015JG003067

Tesi, T., Semiletov, I., Hugelius, G., Dudarev, O., Kuhry, P., & Gustafsson, Ö. (2014). Composition and fate of terrigenous organic matter along the Arctic land-ocean continuum in East Siberia: Insights from biomarkers and carbon isotopes. *Geochimica et Cosmochimica Acta*, *133*, 235–256. https://doi.org/10.1016/j.gca.2014.02.045

Vonk, J. E., Mann, P. J., Davydov, S., Davydova, A., Spencer, R. G. M., Schade, J., et al. (2013). High biolability of ancient permafrost carbon upon thaw. *Geophysical Research Letters*, *40*(11), 2689–2693. https://doi.org/10.1002/grl.50348

Vonk, J. E., Sánchez-García, L., Semiletov, I., Dudarev, O., Eglinton, T., Andersson, A., & Gustafsson, O. (2010). Molecular and radiocarbon constraints on sources and degradation of terrestrial organic carbon along the Kolyma paleoriver transect, East Siberian Sea. *Biogeosciences*, *7*(10), 3153–3166. https://doi.org/10.5194/bg-7-3153-2010

Wakeham, S. G., Canuel, E. A., Lerberg, E. J., Mason, P., Sampere, T. P., & Bianchi, T. S. (2009). Partitioning of organic matter in continental margin sediments among density fractions. *Marine Chemistry*, *115*(3–4), 211–225. https://doi.org/10.1016/j.marchem.2009.08.005

Winterfeld, M., Goñi, M. A., Just, J., Hefter, J., & Mollenhauer, G. (2015). Characterization of particulate organic matter in the Lena River delta and adjacent nearshore zone, NE Siberia - Part 2: Lignin-derived phenol compositions. *Biogeosciences*, *12*(7), 2261–2283. https://doi.org/10.5194/bg-12-2261-2015

Winterfeld, M., Laepple, T., & Mollenhauer, G. (2015). Characterization of particulate organic matter in the Lena River delta and adjacent nearshore zone, NE Siberia - Part I: Radiocarbon inventories. *Biogeosciences*, *12*(12), 3769–3788. https://doi.org/10.5194/bg-12-3769-2015

Yunker, M. B., Macdonald, R. W., Cretney, W. J., Fowler, B. R., & McLaughlin, F. A. (1993). Alkane, terpene and polycyclic aromatic hydrocarbon geochemistry of the Mackenzie River and Mackenzie shelf: Riverine contributions to Beaufort Sea coastal sediment. *Geochimica et Cosmochimica Acta*, *57*(13), 3041–3061. https://doi.org/10.1016/0016-7037(93)90292-5